

EFFECTS OF ANISOTROPIC THERMAL CONDUCTION ON X-RAY EMISSION FROM SNRS

P. F. Velázquez, J. Martinell, and A. C. Raga

Instituto de Ciencias Nucleares, Universidad Nacional Autónoma de México

RESUMEN

Diversos mecanismos físicos han sido estudiados para explicar la morfología mixta (tipo cáscara en radio y centro lleno en rayos X) de algunos remanentes de supernova (RSN). Uno de los mecanismos propuestos es la conductividad térmica, la cual evitaría la caída abrupta de la densidad central del remanente aumentando de este modo la emisión en rayos X de las regiones centrales de los RSN. En este trabajo presentamos simulaciones numéricas con simetría axial, en las que hemos incluido la inducción del campo magnético y la conductividad. Hemos realizado comparaciones entre los resultados obtenidos considerando la conductividad anisótropa y el caso sin conducción. También hemos generado mapas simulados de la emisión en rayos X, de manera de poder comparar los resultados numéricos con las observaciones.

ABSTRACT

Several physical mechanisms have been studied in order to explain why composite supernova remnants (SNRs) have shell-like morphologies in radio continuum while their X-ray emission is centrally peaked. One of the proposed mechanisms has been the presence of thermal conduction, which can raise the density at the center of SNRs, increasing the X-ray emission from these regions. In this work, we have carried out axisymmetric numerical simulations with the adaptive grid yguazú-a code, including the advection of the magnetic field and the thermal conduction. We have considered cases with anisotropic thermal conduction, as well as with no conduction. We have simulated X-ray emission maps from our numerical simulations for these both cases, and we then compare these predictions with recent X-ray observations of SNRs.

Key Words: ISM: MAGNETIC FIELDS — ISM: SUPERNOVA REMNANTS — METHODS: NUMERICAL — X-RAYS: ISM

1. INTRODUCTION

Supernova remnants (SNRs) can be classified by their shapes or morphologies in radio and X-ray emission as shell-like, Crab-like or plerionic, composite or thermal X-ray composite. The SNRs of this last type are characterized by having centrally peaked X-ray emission, while at the same time having a shell-like morphology at radio frequencies. As examples of this kind of SNR, we can mention SNR W 28 (Dubner et al. 2000), W 44 (Giacani et al. 1997), and 3C 400.2 (Dubner et al. 1994; Giacani et al. 1998).

Several authors have given different models in order to explain the centrally peaked X-ray emission from composite SNRs (White & Long 1991; Hnatyk & Petruk 1999; Petruk 2001). An interesting mechanism was proposed by Shelton et al. (1999) and Cox et al. (1999). They consider that isotropic thermal conduction can maintain a high density central region in a SNR, producing centrally peaked X-ray emission. However, if a magnetic field is present the

thermal conduction occurs exclusively in the direction parallel to the \mathbf{B} -field and a breakdown of the initial spherical symmetry of the flow is produced (Zhekov & Myasnikov 2000 considered this for stellar wind studies).

In the present work, we present two-dimensional, axisymmetric numerical simulations of the evolution of SNRs, in which the anisotropic thermal conduction has been included. From our models, we have generated X-ray maps in order to compare our numerical results with the new observations obtained with X-ray satellites such as *Chandra*.

2. INITIAL CONDITIONS AND ASSUMPTIONS

2.1. The Model

The axisymmetric simulations were carried out with the yguazú-a code, which is described in detail in Raga, Navarro-González, & Villagrán-Muniz (2000). In our models we have included a magnetic field, which is initially homogeneous (in modulus and direction). The Lorentz force of the magnetic field on the gas has not been included.

We have then integrated the cylindrically symmetric gas dynamic equations, the induction equation for the magnetic field, and a series of rate equations for different atomic/ionic species. A 6-level binary adaptive grid with a maximum resolution of 2.34×10^{17} cm was employed, in a 40×40 pc (axial \times radial) computational domain.

We have modeled the initial remnant as a sphere centred on the origin of the (x, r) coordinate system within which we impose the Sedov solution with an energy of 10^{51} erg, and with an initial radius $r_0 = 2.5 \times 10^{18}$ cm. The material within the initial remnant is assumed to be fully ionized. The remnant expands into a uniform, neutral (except for C which is singly ionized) environment having a number density of 6 cm^{-3} and a temperature of 1000 K. The initial magnetic field has a strength of $1 \mu\text{G}$ and is parallel to the symmetry axis of the computational grid. Even though this initial configuration for \mathbf{B} is not realistic, it does not affect the results obtained, as it is rapidly advected outwards, forcing it to take the configuration appropriate for an expanding bubble of hot gas.

2.2. Thermal Conduction Treatment

When a magnetic field \mathbf{B} is present, the thermal conduction is anisotropic, taking the form: $q_{\parallel}^e = -\kappa_{\parallel}^e \nabla_{\parallel} T$ where $\nabla_{\parallel} T = [(\hat{\mathbf{B}} \cdot \nabla)T]\hat{\mathbf{B}}$ is the temperature gradient parallel to the magnetic field. The more accurate expression for the parallel thermal conductivity is $\kappa_{\parallel}^e = 3.2nk^2T\tau_e/m_e$ (Braginskii 1965), where n is the electron number density, k is the Boltzmann constant, m_e is the electron mass and $\tau_e = 0.275(T_e^{3/2})/(n\Lambda)$ s is the electron collision time. $\Lambda = 24 - \ln(n^{1/2}T^{-1})$ is the Coulomb logarithm for electron-electron collisions.

However, the expression given above for q_{\parallel}^e is no longer valid when the electron mean-free-path λ_e is larger than the temperature scale height $L_T = T/|\nabla T|$. In this case, a saturation of the heat flux is produced, which was studied by Cowie & McKee (1977) for the non-magnetic case. Generalizing their results, we can give the following expression for the anisotropic saturated heat flux $q_{\parallel, \text{sat}} = -\text{sgn}(\mathbf{B} \cdot \nabla T)5\phi_s cP\hat{\mathbf{B}}$. Here ϕ_s is a factor reducing thermal conduction of the order of 1. For the SNR case it is usually set to 0.3.

In the following sections we present simulations of SNRs with and without thermal conduction and considering non-saturated and saturated heat flux (i.e., $\lambda_e < L_T$ and $\lambda_e > L_T$, respectively).

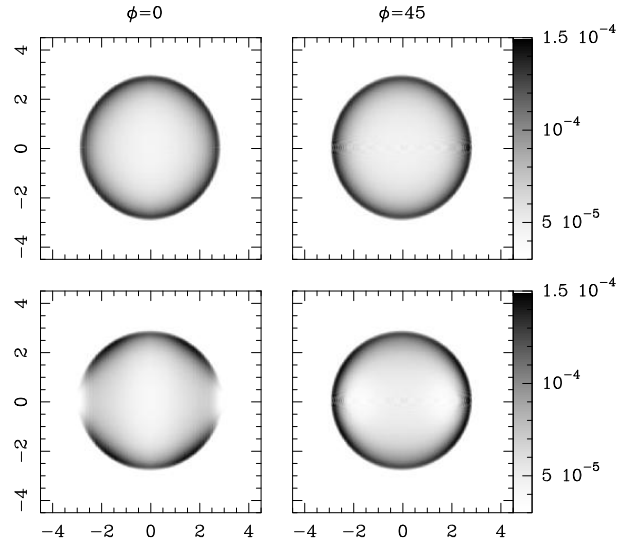


Fig. 1. X-ray maps obtained by integrating the X-ray emission coefficient along the line of sight. The top and bottom panels show the emission for the no conduction and anisotropic conduction cases, respectively, after 21,000 yr of evolution. The left column shows the X-ray emission considering an angle of $\phi = 0^\circ$ with respect to the line of sight, while the right column shows the same for an angle of 45° . The scales of the x - and y -axes are given in units of 10^{19} cm. The grayscale of the X-ray emission is linear.

3. RESULTS

Figure 1 shows simulated X-ray maps for a $t = 21,000$ yr integration time, which were obtained by integrating the emission coefficient (in the 0.3 to 10 keV energy range) along lines of sight. In the left column of the figure we have X-ray emission maps for the anisotropic and no conduction cases (bottom and top panels, respectively) when the angle with respect to the plane of the sky is $\phi = 0^\circ$, while the right column shows the same maps, but considering a $\phi = 45^\circ$ angle.

We notice that the X-ray emission for the case with no thermal conduction exhibits a typical shell-like morphology for the maps obtained at $\phi = 0^\circ$ and $\phi = 45^\circ$. (top panels, Fig. 1). The maps for the anisotropic conduction case (bottom panels, Fig. 1) show significant differences between the two considered projection angles. For $\phi = 0^\circ$, the X-ray emission shows an incomplete shell, with bright edges away from the symmetry axis. Along the symmetry axis, the outer emission shell disappears completely. This morphology changes into a complete shell with diffuse internal emission, which has two symmetric minima (along the x -axis, Fig. 1) for $\phi = 45^\circ$.

4. CONCLUSIONS

In this work we compare simulated X-ray emission maps of a SNR for the cases with anisotropic and no thermal conduction. We have also taken into account how projection effects can modify the morphology of the remnant in both the X-ray and the radio continuum emission.

From our simulations we see that thermal conduction has noticeable effects on the X-ray emission (see Fig. 1). Even for the simple initial magnetic field configuration that we have assumed, we find that anisotropic conduction leads to complex, fragmented shell morphologies for the predicted X-ray maps.

Finally, we find that in the calculations with anisotropic conduction, we do not obtain centrally peaked X-ray emission maps, such as the ones obtained from simulations with isotropic conduction (see Fig. 1, Cox et al. 1999 and Shelton et al. 1999). From this result, we tentatively conclude that the centrally peaked X-ray morphologies observed in some SNRs (see e.g., Dubner et al. 2000) cannot be explained in terms of a model of a SNR expanding into a uniform environment, even if the effect of the electron thermal conduction is included in an appropriate way (i.e., considering the effect of the magnetic field on the conduction).

AR and PV acknowledge financial support from CONACyT grants 34566-E and 36572-E. JM is supported by grant IN116200 DGAPA-UNAM. We thank Israel Díaz for computing support.

REFERENCES

- Braginskii, S. I. 1965, *Reviews of Plasma Physics*, 1, 205
 Cox, D. P., et al. 1999, *ApJ*, 524, 179
 Cowie, L. L., & McKee, C. F. 1977, *ApJ*, 211, 135
 Dubner, G. M., Giacani, E. B., Goss, W. M., & Winkler, P. F. 1994, *AJ*, 108, 207
 Dubner, G. M., Velázquez, P. F., Goss, W. M., & Holdaway, M. A. 2000, *AJ*, 120, 1933
 Giacani, E. B., Dubner, G., Cappa, C., & Testori, J. 1998, *A&AS*, 133, 61
 Giacani, E. B., et al. 1997, *AJ*, 113, 1379
 Hnatyk, B., & Petruk, O. 1999, *A&A*, 344, 295
 Petruk, O. 2001, *A&A*, 371, 267
 Raga, A. C., Navarro-González, R., Villagrán-Muniz, M. 2000, *RevMexAA*, 36, 67
 Shelton, R. L., et al. 1999, *ApJ*, 524, 192
 White, R. L., & Long, K. S. 1991, *ApJ*, 373, 567
 Zhekov, S. A., & Myasnikov, A. V. 2000, *ApJ*, 543, L53